Ocean Modelling 35 (2010) 304–313

Contents lists available at ScienceDirect

Ocean Modelling

journal homepage: www.elsevier.com/locate/ocemod

The effect of ocean tides on a climate model simulation

M. Müller [a,b,*], H. Haak [a], J.H. Jungclaus [a], J. Sündermann [c], M. Thomas [d]

[a] Max Planck Institute for Meteorology, Bundesstr. 53, 20146 Hamburg, Germany
[b] University of Victoria, School of Earth and Ocean Sciences, P.O. Box 1700 Stn Csc, Victoria, Canada V8W2Y2
[c] University Hamburg, Institute of Oceanography, Bundesstr. 53, 20146 Hamburg, Germany
[d] German Research Centre for Geosciences, Telegrafenberg, 14473 Potsdam, Germany

ARTICLE INFO

Article history:
Received 28 January 2010
Received in revised form 19 August 2010
Accepted 2 September 2010
Available online 16 September 2010

Keywords:
Ocean tides
Tidal mixing
North Atlantic Current
Western European Climate

ABSTRACT

We implemented an explicit forcing of the complete lunisolar tides into an ocean model which is part of a coupled atmosphere–hydrology–ocean–sea ice model. An ensemble of experiments with this climate model shows that the model is significantly affected by the induced tidal mixing and nonlinear interactions of tides with low frequency motion. The largest changes occur in the North Atlantic where the ocean current system gets changed on large scales. In particular, the pathway of the North Atlantic Current is modified resulting in improved sea surface temperature fields compared to the non-tidal run. These modifications are accompanied by a more realistic simulation of the convection in the Labrador Sea. The modification of sea surface temperature in the North Atlantic region leads to heat flux changes of up to 50 W/m^2. The climate simulations indicate that an improvement of the North Atlantic Current has implications for the simulation of the Western European Climate, with amplified temperature trends between 1950 and 2000, which are closer to the observed trends.

1. Introduction

In the last decade ocean tides have returned into the focus of attention in oceanographic research. Theoretical and observational estimates support the hypothesis that a considerable amount of energy is transferred from tidal currents into mixing processes of the oceans (Munk and Wunsch, 1998; Egbert and Ray, 2000). These findings suggested that it is necessary to allow for an interactive approach of ocean tides and ocean circulation.

In climate modelling the consideration of ocean tides failed to appear due to considerably different time scales of climate and tidal models, numerical stability problems, and due to the “rigid lid” condition often used in the ocean component of climate models (see Schiller (2004) for more details). So far, three global Ocean General Circulation Models (OGCMs) are existing, which explicitly include ocean tides: (1) Thomas et al. (2001) extended an OGCM by implementing the complete lunisolar tidal forcing. (2) Schiller and Fiedler (2007) described the implementation of the forcing of eight tidal constituents in an OGCM and their influence on transport and mixing processes in the Indonesian Seas and off the Australian Northwest Shelf. Finally, (3) a recent study by Arbic et al. (2010) included a forcing of the major tidal constituents in a high-resolution eddy resolving ocean model. The processes of tidal mixing are unresolved in OGCMs and must be parameterized, even when tides are forced explicitly. In shelf regions, where strong tidal currents occur, mixing is generated by enhanced vertical velocity in the bottom boundary layer. In the deep ocean tidal mixing is caused by the generation and breaking of internal waves over rough topography (Garrett, 2003). Tidal mixing in the deep ocean is usually considered by a parameterization depending on roughness of the ocean topography, on vertical stratification and on the magnitude of tidal currents (Simmons et al., 2004; Montenegro et al., 2007). To allow for tidal mixing in shelf regions Lee et al. (2006) included tidal currents of an external ocean tide model into their Richardson number dependent vertical mixing scheme. In another approach Bessières et al. (2008) included the ocean tidal residual mean circulation, obtained from an tide-only model, into a global climate model. Detailed studies of locally enhanced mixing on the general ocean circulation can be find in Saenko (2006) and Jayne (2009).

In the present study we implemented the tidal module developed by Thomas et al. (2001) in a climate model which was used for the Intergovernmental Panel on Climate Change (IPCC) fourth assessment report simulations. Thus, tides are forced explicitly and tidal mixing is realized in the ocean model by tidal currents inducing vertical shear of velocity through bottom friction, which in turn acts on the vertical mixing scheme. This approach generates tidal mixing mainly on the continental shelf and not in the deep ocean. The next step will be to implement an additional parameterization of tidal mixing generated by internal wave breaking (St.-Laurent et al., 2002) and will be subject to future research. In addition to mixing the tidal currents interact with low frequency

* Corresponding author at: University of Victoria, School of Earth and Ocean Sciences, P.O. Box 1700 Stn Csc, Victoria, Canada V8W2Y2. Tel.: +1 250 472 4008.
E-mail address: mmueller@uvic.ca (M. Müller).

1463-5003/$ - see front matter © 2010 Elsevier Ltd. All rights reserved.
doi:10.1016/j.ocemod.2010.09.001

motions through nonlinear bottom friction and act on the vertical viscosity parameterization scheme of the model.

The goal of the present study is to present an ensemble of climate model experiments with an explicit lunisolar tidal forcing. The results show that the effect of tides through mixing and nonlinear interactions have a significant influence on the climate model simulations. Further, this study demonstrates that it is possible to obtain global tidal patterns in an OGCM with an accuracy comparable with classic barotropic non-constrained tidal models. In Section 2 we give a brief description of the model and the setup of the experiments. Section 3 describes the tidal patterns and their accuracy and in Section 4 we show how physical quantities are modified by tides in the model. In Section 5 we describe the impact of tides on current and water mass properties in the North Atlantic. Since the sea surface temperature and ocean–atmosphere heat flux in the North Atlantic is changed on large scales, a significant secondary effect occurs in the atmospheric component of the climate model (Section 6).

2. Model description

The climate model is the coupled atmosphere–hydrology–ocean–ice model of the Max Planck Institute for Meteorology (ECHAM5/MPI-OM) (Jungclaus et al., 2006). The Max Planck Institute Ocean Model (MPI-OM) is extended by an explicit forcing of the complete lunisolar tides (Thomas et al., 2001). In this real-time approach the tidal potential is deduced from lunisolar ephemerides according to the instantaneous positions of moon and sun. The loading and self-attraction is not considered in the ocean circulation model. The time resolution of the ocean model is 2160 s. The time-step of the ocean model is reduced compared to the original value used for the IPCC AR4 simulations (4800 s) for the reliable representation of semi-diurnal and diurnal ocean tides. The ocean model utilizes horizontally a bipolar orthogonal grid where the positions of the north and south pole can freely be chosen. In this configuration the grid North Pole is centered on Greenland, which leads to an increased resolution for the North Atlantic region (near Greenland up to 12 km). Vertically the grid has 40 layers. A detailed description of the model is given by Marsland et al. (2003). The atmosphere model is the European Center/Hamburg model version 5 (ECHAM5) and it is run at T63L31 resolution (Roeckner et al., 2003). Atmosphere and ocean are coupled without flux correction by means of the OASIS coupler (Valcke, 2006). Six coupled experiments have been performed, one control run without the tidal potential and an ensemble of five experiments with the consideration of the lunisolar tides. The latter only differ in their initial conditions, which are taken in one hundred year intervals from the 500 year IPCC AR4 pre-industrial control run. The simulations cover the period 1860–2000 and are forced by observed greenhouse gas emissions and pre-calculated sulfate aerosols.

In the following sections we compare the ensemble means of the experiments with tides with the control run without tides. Figures, which show vertically integrated ocean currents are based on one particular ensemble member and are averaged over 10 years. Due to the high temporal variability of the ocean currents the illustration of ensemble mean, or averaged over a longer period, current vectors would blur the pathway of the currents. However, for the scalar variables like sea surface temperature, mixed layer depth and ocean–atmosphere heat flux, we show ensemble mean values averaged over a period of 50 years. Diagnostic quantities, as tidal velocity, bottom friction dissipation, vertical diffusivity and viscosity are based on model output of a particular year and ensemble member.

3. Evaluation of tidal patterns

In this section the main semi-diurnal and diurnal tidal patterns in the climate model are evaluated. It is meaningful to evaluate both, tidal velocities and elevations, since the focus of the present study is on the effect of tides on the ocean circulation model, and this effect is mainly caused by tidal velocities rather than by tidal elevations. The strongest tidal currents occur in shallow waters where current tide models have their largest uncertainties (Shum et al., 1997). Even with modern techniques of assimilating data into tide models the residuals of tidal velocities are still large in shallow waters. Evaluations of tidal currents of barotropic tide models are rare and most of the comparisons with observational data has been done so far in the deep ocean (Ray, 2001). In the following, we compare qualitatively tidal currents with the model of Zahel et al. (2000) (Z2000), which determines tidal velocities by assimilating satellite data in a numerical hydrodynamical model. Tidal elevation fields are compared quantitatively with the observational pelagic ST103 dataset (LeProvost, 1994).

The tidal constituents of the ocean tides, can be obtained from the model output by means of harmonic analyzes (e.g., Emery and Thompson, 1998). The simulated global sea surface elevation and barotropic velocity pattern of every time-step (2160 s) over one arbitrary model year are used for harmonic analyzes. This is a sufficient time resolution and record length to resolve the main semi-diurnal and diurnal tidal constituents. A quantitative comparison of the tidal patterns with the observational pelagic ST103 dataset (LeProvost, 1994) is obtained by computing the RMS errors of the tidal amplitudes:

$$\mathrm{RMS} = \sqrt{\frac{1}{103}\sum_{i=1}^{103}\left(A_i^{Model} - A_i^{\mathrm{ST103}}\right)^2}. \tag{1}$$

Here, A_i^{Model} and A_i^{ST103} are the amplitudes of a tidal constituent at the ith-station in the model and at the tide gauge, respectively. The RMS errors are 12.9 cm for M_2 and 4.8 cm for K_1. These values are, of course, much larger than those of model approaches with assimilation of satellite data which have RMS errors in the range of just a few centimeters, even for the M_2 tide (Shum et al., 1997). Also, a model without assimilation of data (Arbic et al., 2004) shows smaller RMS errors. However, this model has (1) higher horizontal resolution of 0.5°, (2) it considers an internal wave drag (conversion of barotropic tide energy into internal waves) and (3) it has a proper treatment of the loading and self-attraction effect. The accuracy of the tidal patterns simulated by the climate model are comparable with classic barotropic tide model approaches without the consideration of internal wave drag and loading and self-attraction effect.

The amplitudes of the tidal velocities of the M_2 and K_1 constituents of the climate model and of the model of Z2000 are shown in Fig. 1. The main patterns of the velocities are similar. However, in detail there are significant differences between the models, most notably in coastal regions. For example the M_2 tidal currents of Z2000 are larger on the European Shelf, Patagonian Shelf, and in the Bering Sea. Instead K_1 tidal currents of Z2000 are smaller in the Southern Ocean and South China Sea. As already stated in the beginning of this section, there is a large uncertainty of tidal velocities in tide models, especially in shallow waters. As the main tidal patterns of Z2000 and the present ocean circulation model are qualitatively consistent, we conclude that the accuracy is high enough for a further analyzes of the effect of tidal currents on the ocean circulation.

For future studies it will be necessary to include a parameterization of the generation of internal waves and to consider the self-attraction and loading effect, in order to obtain improved tidal patterns. However, the discrepancies between observations and model will have a minor relevance in the following analysis of climate relevant variables.

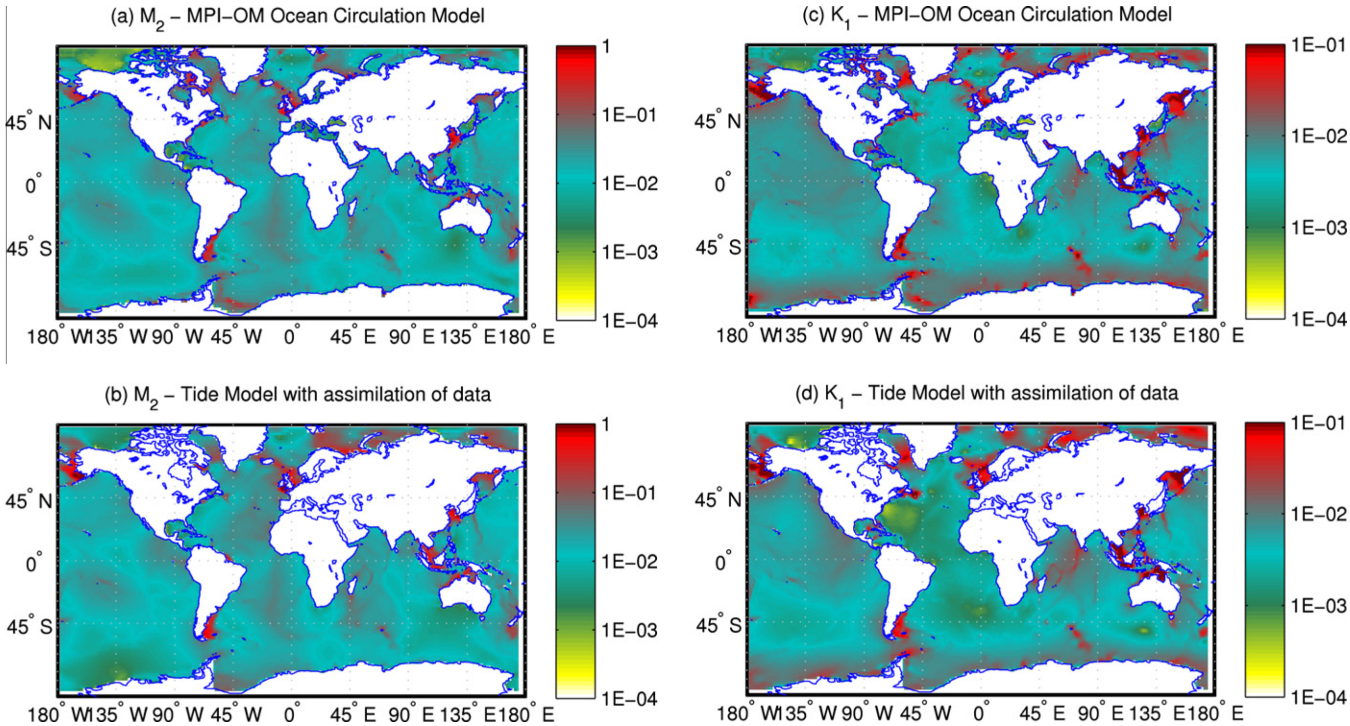

Fig. 1. Barotropic tidal velocities in [m/s]. The M_2 and K_1 constituents in the OGCM (a), (c) and of the reference model Z2000 (b), (d) are shown.

4. Physical quantities affected by tidal currents

The physical quantities which are directly influenced by the tidal currents are the vertical diffusivity, vertical viscosity and nonlinear bottom friction. The vertical diffusivity and viscosity are parameterized in the OGCM with a Richardson number dependent term, following Pacanowski and Philander (1981). The Richardson number is given by

$$Ri = \frac{N^2}{\left(\frac{\partial U}{\partial z}\right)^2}, \tag{2}$$

N is the Brunt–Väisälä frequency and $\frac{\partial U}{\partial z}$ the vertical velocity shear. The diffusivity A_V and the viscosity K_V in the model are defined as

$$A_V = A_{V0}(1 + C_A \cdot Ri)^{-3} + A_b + A_w, \tag{3}$$

$$K_V = K_{V0}(1 + C_K \cdot Ri)^{-2} + K_b + K_w, \tag{4}$$

where A_{V0}, K_{V0}, C_A, and C_K are constants, A_b (K_b) is a small constant background diffusivity (viscosity) and A_w (K_w) is the diffusivity (viscosity) generated by the wind at the sea surface. Through the presence of tidal velocities, the vertical velocity shear increases in the bottom layer through bottom friction. Thus, in regions of high tidal velocities (e.g. at the European shelf, see Fig. 2) the inverse Richardson number becomes up to ten times larger due to the velocity shear induced by strong tidal currents. In Fig. 2 the vertical diffusivity depth-profile is shown at a grid point close to the European shelf (11°W/52°N) and for the global averaged values. It indicates that the vertical mixing is amplified locally through tides, but the global mean value of the diffusivity is only slightly changed. In the depth range of about 800–2400 m the diffusivity is even slightly reduced when considering tides. This is due to a secondary effect of tides. The tides change for example the pathway of the warm and salty North Atlantic Current (Section 5) and associated with that, the vertical and horizontal distribution of water masses on large scales gets changed. This in turn leads to changes in the stratification, which induces changes in the vertical diffusivity.

Further, global maps of vertical diffusivity and viscosity in the bottom boundary layer are shown in Fig. 3. They indicate the regions where the tidal velocities mainly act on the vertical diffusivity and viscosity scheme. As expected the main influence is in shallow waters where the tidal velocities are strongest.

Apart from the 'physical' diffusivity, 'spurious' (numerical) diffusivity is generated by the advection scheme and the vertical tidal velocities. To estimate the magnitude of tide induced spurious diffusivity, the vertical velocities of the eight main semi-diurnal and diurnal constituents (N_2, M_2, S_2, K_2, K_1, O_1, P_1, and Q_1) are computed by means of harmonic analyzes of a particular year of the simulation. Hence, the maximum of vertical tidal velocity w_t is defined as the sum of the amplitude of the velocities of all eight tidal constituents. We estimated the upper bound of numerical diffusivity by the product of the maximum vertical tidal velocity w_t and the layer thickness Δz (Griffies et al., 2000). Compared to the explicit diffusivity A_V induced by ocean tides the upper bound of spurious diffusivity $w_t \Delta z$ is at most locations more than one order of magnitude lower. There are only a few locations, where the numerical diffusivity exceeds A_v, which is close to steep topographical features.

Further, the tidal velocities act on the nonlinear bottom friction parameterization in the model

$$F_B = c_d \cdot u_B |u_B|, \tag{5}$$

where u is the velocity in the bottom boundary layer and c_d the bottom drag coefficient with a value of 0.003. To give a qualitative estimate of the inferred bottom friction through the tides the mean energy dissipated by bottom friction

$$W_B = \langle \rho c_d \cdot |u_B^3| \rangle \tag{6}$$

is shown in Fig. 4. The brackets $\langle\rangle$ denote time averaging, ρ is the mean density (1035 kg/m^3), and u_B are the velocity amplitudes in the lowest layer of the OGCM. The amount of energy dissipated through bottom friction is the integral of W_B over the global ocean and it yields 2.4 TW and 0.6 TW for the experiments with and without tides, respectively. Thus, through inclusion of tides 1.8 TW of

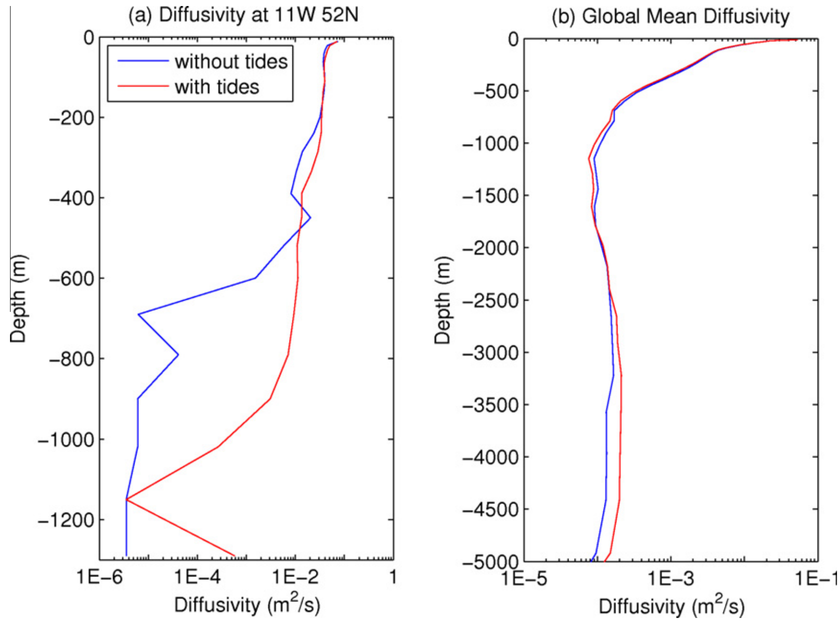

Fig. 2. The depth-profiles of the vertical diffusivity A_V in [m^2/s] for a grid point on the European shelf (a) and the global averaged values (b). The blue and red lines represent the control run without tidal forcing and one ensemble member with tidal forcing, respectively. (For interpretation of the references to color in this figure legend, the reader is referred to the web version of this article.)

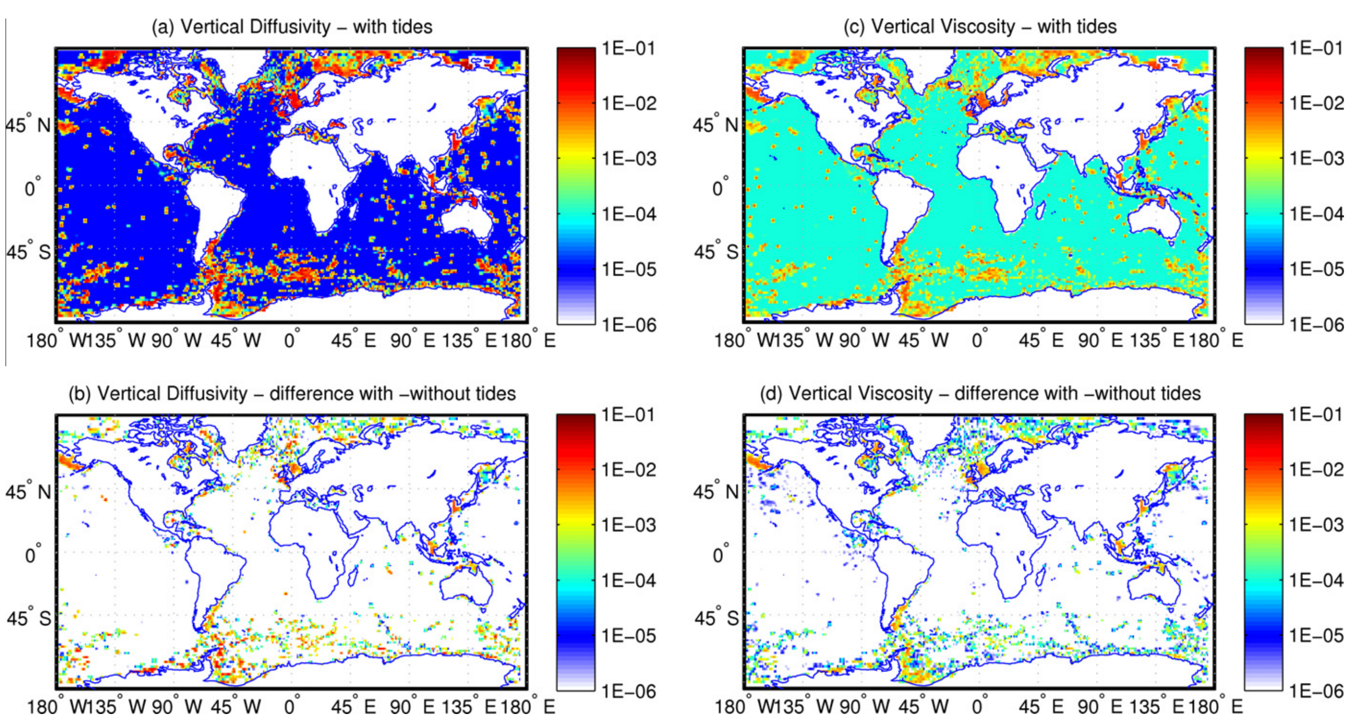

Fig. 3. Global maps of vertical diffusivity and viscosity [m^2/s] in the bottom layer of the OGCM. The diffusivity and viscosity of an experiment with tides are shown in (a) and (c), respectively. The difference in diffusivity and viscosity between an experiment with tides and the control run without tides are shown in (b) and (d), respectively.

energy are additionally dissipated through bottom friction. Estimates of barotropic tide models give values of around 1.8 TW for M_2 only (Lyard et al., 2006), thus the dissipated energy in the ocean circulation model is lower than in tide-only models. The value of 0.6 TW of energy dissipated by the non-tidal flows is consistent with recent model and observational dissipation estimates of 0.1–0.8 TW (Arbic et al., 2009).

5. The impact of tides on ocean circulation

The horizontal tidal velocities are very large in the North Atlantic (Fig. 1) and thus there is a large amount of induced tidal mixing and nonlinear interaction through bottom friction between the tidal currents and the low frequency motion. In the following of our study we will focus on the ocean circulation properties in the

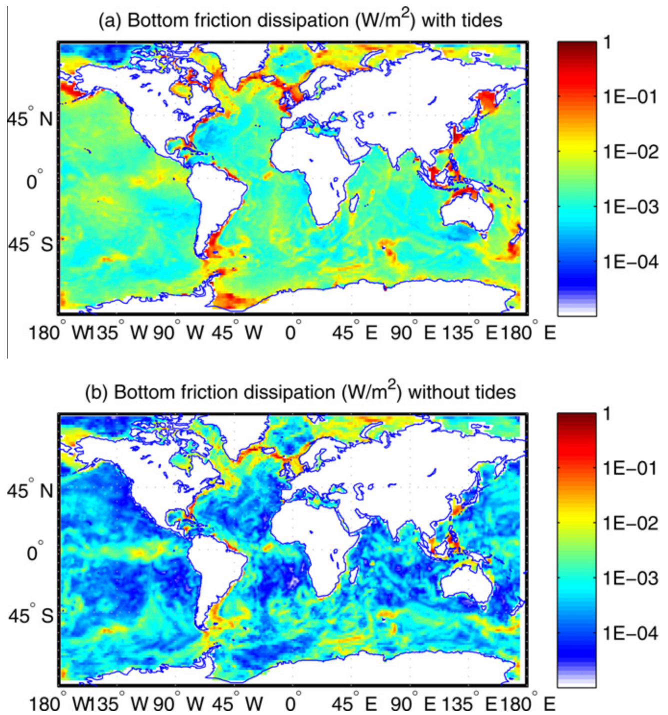

Fig. 4. Bottom friction dissipation rate [W/m^2] of the experiments with tides (a) and without tides (b).

North Atlantic region. The dynamics in the upper layer of the North Atlantic are primarily determined by the North Atlantic Current (NAC). This wind driven boundary current transports heat from tropical towards northern latitudes. The NAC has its source in the Gulf Stream, which divides into two branches at the southeast of the Grand Banks; the northern branch is the NAC and the southern one the Azores Current. The branching area is characterized by high temporal variability caused by the formation and decay of eddies in this region. Depending on the eddy locations and sense of rotation the branching has a time varying preferential direction, either towards the north into the NAC or to the east into the Azores Current (Käse and Krauss, 1996). Towards the north, the NAC is trapped by the continental slope along the Grand Banks and at 49°N, north-east of Flemish Cap, it passes northward into the Northwest Corner at 51°N. Further downstream the NAC meanders in north-east direction across the Atlantic.

The described pathway of the NAC is not properly represented in coarse resolution models, which are used for climate predictions (IPCC, 2007, p. 614). A common error in these models is a minor pronunciation of the branching of the Gulf Stream in the region southeast of the Grand Banks. Instead of flowing northward along the continental slope, the NAC crosses the Atlantic too zonally at about 40°N. Thus, the subpolar front, the transition of warm and saline sub-tropical water masses and cold and fresh subpolar water masses is misrepresented, which leads to a large temperature bias in the middle of the North Atlantic. The representation of the NAC and the associated subpolar front depends on various model factors. For example Böning et al. (1996) obtained a strong improvement when using an eddy-resolving model. In their model the subpolar front gets sharper and shifted to the north due to the resolving of eddies. Further, the Gulf Stream and the NAC along the continental slope depend on the Deep Western Boundary Currents, which emphasizes the importance of the representation of the Denmark Strait overflow water (Gerdes and Köberle, 1995). As well, Döscher et al. (1994) showed that the course of the NAC east of 45°W strongly depends on the representation of the Denmark Strait overflow waters.

In our model the NAC spuriously crosses the Atlantic zonally at 40–45°N and thus the model has a strong negative SST bias in the middle of the northern Atlantic. The SST deviations from observations are up to 5°. Further, the NAC transports, due to its wrong pathway, too much heat towards the Nordic Seas and the Barents Sea and as a result, the SST in these regions is too warm (Fig. 5).

The experiments with ocean tides show a modified and improved pathway of the NAC. In the control run without ocean tides, the NAC flows in eastward direction after it originates in the branching area at the southeast corner of the Grand Banks (Fig. 6). In the experiments with tides the NAC flows northward along the continental slope. At approximately 46°N the NAC branches into an eastward and a northward directed current. The major part flows eastward and the remaining northward flow builds the Northwest Corner. Although the strength of this northward extension is still too weak, the adjustment of the NAC in its source region improves the pathway further downstream east of 45°W and improves the SST on large scales in the North Atlantic by up to 3°. This is due to the fact that part of the heat is diverted to the middle of the southern North Atlantic. This heat is missing on its continuing pathway and thus the Nordic Seas, especially the Norwegian Sea, and the Barents Sea are cooler with more realistic SST values than in the model without tides (Fig. 5). However, there are also areas where the SST values are getting worse, which indicates that the NAC's pathway is still not correct.

The adjustment of the pathway of the NAC improves not only the SST in the North Atlantic but the dynamical system in that region. Since the subpolar front is shifted to the north, the

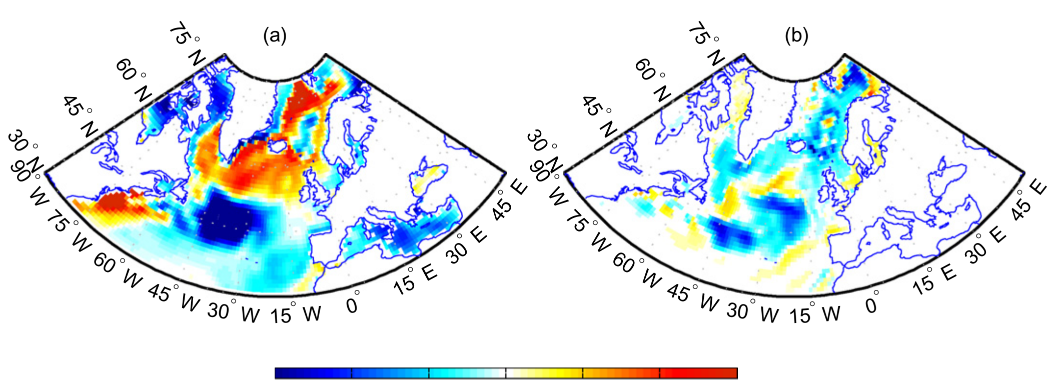

Fig. 5. Sea surface temperature in the North Atlantic region (time mean 1950–1999). (a) Difference (ΔT) between observational data (Steele et al., 2001) and control run without tides. (b) Difference between ΔT with tides and without tides (95% significance level).

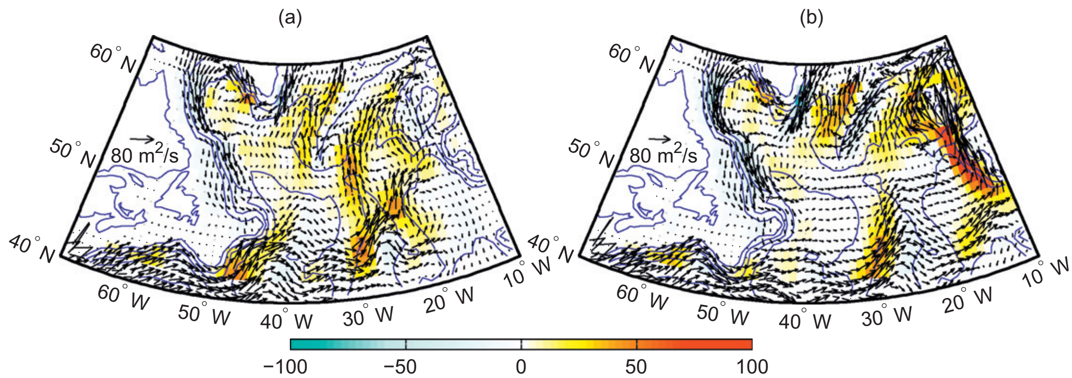

Fig. 6. Vertically integrated (0–640 m) currents [m^2/s] (1970–1979). The meridional velocities are color contoured, positive (negative) values depict northward (southward) transports. (a) Experimental run with tidal forcing (b) control run without tidal forcing. (For interpretation of the references to color in this figure legend, the reader is referred to the web version of this article.)

representation of the recirculation of the Labrador Current is improved, which modifies the transport of cold and fresh water back to the Labrador Sea. This has implication on the features of the Labrador Sea Water (LSW) which is formed in that region. The LSW gets fresher and thus compares better with observations (Fig. 7). The improvement of the water mass properties of LSW induced by an adjustment of the NAC is consistent with recent results of Weese and Bryan (2006). Moreover, these results coincide with that of Lee et al. (2006). They also obtained improved salinity values in the Labrodor Sea, when adding tidal mixing to a coupled atmosphere–ocean model.

Further, through the northward shift of the subpolar front the extension of the subpolar gyre is modified, which affects the deep-ocean convection. The winter deep-ocean convection in the Labrador Sea, forms the LSW, an intermediate water mass at depths between 1000 and 2300 m. To study the convection process we use the quantity of the mixed layer depth (MLD). In the present study it is defined as the depth at which the density difference from the sea surface is 0.125 sigma units, following Monterey and Levitus (1997). Hence, large values of MLD represent the region where deep-convection takes place. The MLDs in the Labrador Sea during wintertime are shown in Fig. 8. The tides change the simulated deep-convection in the model significantly. When neglecting ocean tides, the region where the MLDs are larger than 1500 m extends from the Labrador Sea south-eastward into the Atlantic ocean, whereas the experiments with ocean tides have their largest MLDs localized in the Labrador Sea at about 58°N, 55°W. Obviously, the northward shifted position of the subpolar front focus the area of deep-convection towards the Labrador Sea. This makes the representation of deep-convection more realistic since observations show similar winter mixed layer depths in the Labrador Sea centered in a small region near 56.5°N, 55°W (Lavender et al., 2000). Another LSW formation site, which is under discussion, was observed in the Irminger Sea (Pickart et al., 2003).

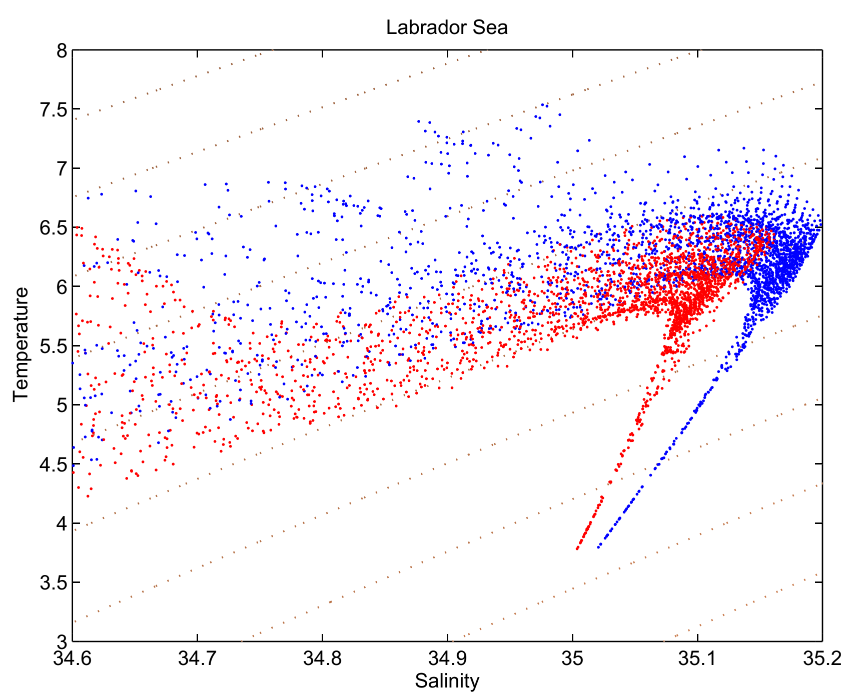

Fig. 7. TS-Diagram of the water masses in the Labrador Sea, defined by a polygon with edges (−55.8W/52.0N; −43.7W/59.9N; −53.7W/66.9N; −64.5W/60.3N). The time mean values (1950–1990) for the ensemble with tides (red) and the control run (blue) are shown. (For interpretation of the references to color in this figure legend, the reader is referred to the web version of this article.)

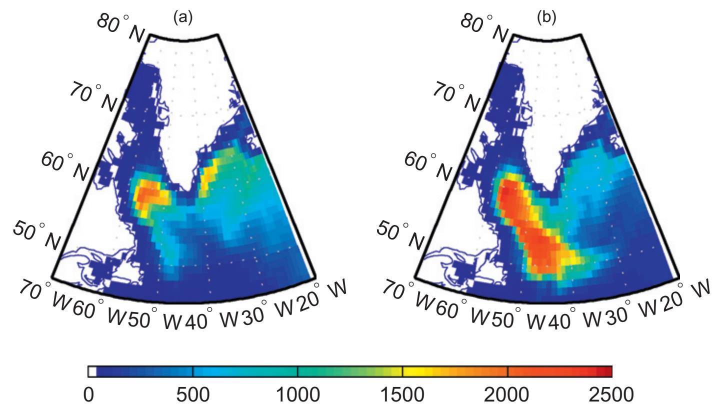

Fig. 8. Maximum monthly mixed layer depth (m). Seasonal (DJF) long term mean (1950–1999). (c) Ensemble mean of five experimental runs with tidal forcing. (d) Control run without tidal forcing.

As well, this deep-convection appears more realistic in the model experiments with tides, represented by a relative maximum of MLD in this region.

As described in Section 4, the tidal currents induce diffusivity, viscosity and nonlinear bottom friction in the shallow waters of the North Atlantic. We assume that the modification of these properties are responsible for the adjustment of the NAC southeast of the Grand Banks, which leads to significant changes in SST in the North Atlantic and to modifications of the deep-convection in the Labrador Sea.

We have two hypotheses on the changes of the NAC. Firstly, tidal currents in the region of the Grand Banks directly affect the NAC dynamics. In this shallow region, strong tidal currents occur and tidal mixing might be effective in a region where the cold and fresh subpolar water meets the warm and saline subtropic waters.

The second hypothesis is, that changes in the Denmark Strait and Faroe Channel overflows are affecting the deep water circulations which in turn change the upper currents. This assumption is based on regional model sensitivity studies of the Gulf Stream and the NAC, which showed that both current systems react sensitive to changes in the deep water currents (Gerdes and Köberle, 1995) and on the representation of the Denmark Strait overflow waters (Döscher et al., 1994). In the model simulations the strength of the Denmark Strait overflow is not significantly changed through the inclusion of tides, instead the placing of the overflow (and also that of the East Greenland Current) is modified. This is illustrated in Fig. 9, where the densities in Denmark Strait are plotted. Obviously, the inclusion of tidal mixing close to the bottom reduces the stratification but has no significant effect on the overflow rates (2.5 ± 0.2 Sv with tides, 2.6 Sv without tides), whereas the deviation represents the standard deviation of all five ensemble members. More obvious is a modification of the overflow pathway, which gets shifted westward. Instead, in the Faroe Bank Channel we have a significantly increased outflow in the experiments with tides. The overflow in the simulations with tides amounts to 1.3 ± 0.3 Sv and in the control experiment without tides the outflow is comparable low with 0.6 Sv. This modification is presumably caused by the changed northward directed flow, i.e. an extension of the NAC, which is weaker in the experiments with tides (3.2 ± 0.3 Sv, between 22°W and 27°W) than in the control experiment without tides (5 Sv). In the control experiment large

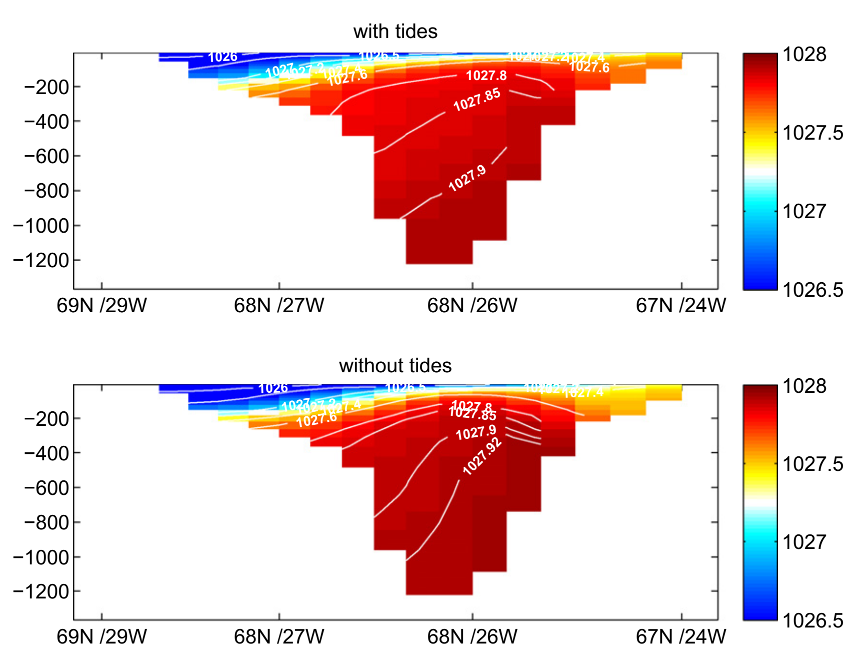

Fig. 9. Vertical section of the Denmark Strait. Long term mean (1950–1999) densities: (a) Experimental run with tidal forcing and (b) Control run without tidal forcing.

amounts of water masses of the NAC spuriously flow northward along the European Shelf (Fig. 6), whereas in the experiments with tides large parts of the NAC meanders in the middle of the Atlantic. This leads to different amounts of northward flow through the Faroe Bank Channel and since the outflow is counterbalanced by the inflow, the outflow rates are larger in the experiments with tides.

These modifications of the overflows, which represent initial states of the North Atlantic Deep Water (NADW) currents, lead to changes in the representation of the NADW pathways (Fig. 10). In the experiments without tides large parts of the NADW flow southward along the transition of the deep ocean to the European Shelf. Instead, in the simulations with ocean tides, the NADW flows along the eastern and western side of the Mid-Atlantic Ridge. Döscher et al. (1994) found in a model study a strong dependence of the strength and location of the deep and upper circulation on the properties of the Denmark Strait overflow waters. Their barotropic streamfunctions (Döscher et al., 1994, Fig. 12) show that the sub-tropical gyre, expands in northward direction east of Grand Banks when changing the overflow properties. Further, they show a deformation of the subpolar gyre, with a stronger focus to the Labrador Sea. Both findings are consistent with our results of the changed pathway of the NAC and the focused MLD towards the Labrador Sea, respectively. This consistency strengthens the hypothesis, that changing nordic overflows control and modify the pathway of the NAC. However, as described above, the simulated flow through the Faroe Bank Channel depends itself on the pathway of the NAC, so it is not clear how one feature affects the other.

6. Resulting effect on the atmosphere

The effect of tides on the pathway of the NAC and the resulting changes in the sea surface temperature, further impact the ocean–atmosphere heat flux. For the North Atlantic region the difference in heat flux between the control run without tides and the ensemble with tides is shown in Fig. 11 (time mean 1950–1999). In the central North Atlantic the simulations differ by values in the range of 50 W/m^2. There, when ocean tides are considered, the heat flux from ocean to atmosphere is enhanced since the NAC transports more heat towards the central North Atlantic. Instead, in the region of the European coast, the heat flux towards the atmosphere is reduced by values of up to 50 W/m^2.

These changes in ocean–atmosphere heat flux induced by the changed pathway of the NAC significantly influence the dynamics of the atmosphere. The dynamical atmospheric patterns are not analyzed in detail, which would be beyond the scope of this paper, but inspired by a recent study of van Oldenborgh et al. (2009) the present temperature trend in Western Europe is analyzed. They showed on the basis of an ensemble of 17 independent climate model simulations (with the same model used in the present study, without tidal forcing) and an intercomparison of current IPCC climate models, that climate models are not able to capture the large present temperature trend observed in Western Europe. They hold the misrepresentation of the NAC in state-of-the-art climate models to some part responsible for the underestimation of the recent temperature trend.

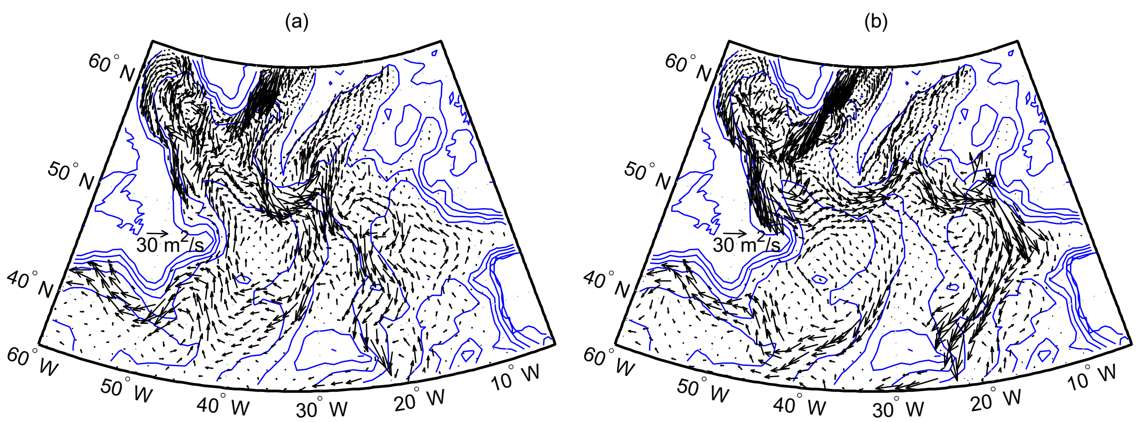

Fig. 10. Vertically integrated (1700 m to ocean bottom) currents [m^2/s] (1970–1979). Vectors are shown for each model grid cell. (a) Experimental run with tidal forcing (b) control run without tidal forcing.

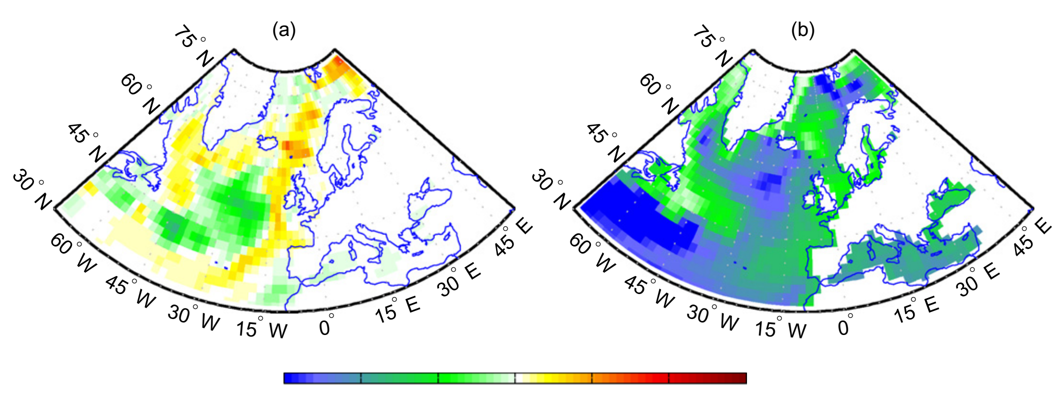

Fig. 11. Heat Flux from atmosphere to ocean (positive) in W/m^2. (a) Difference between ensemble with tides minus control run without tides. (b) Time mean (1950–1999) heat flux of ensemble with tides.

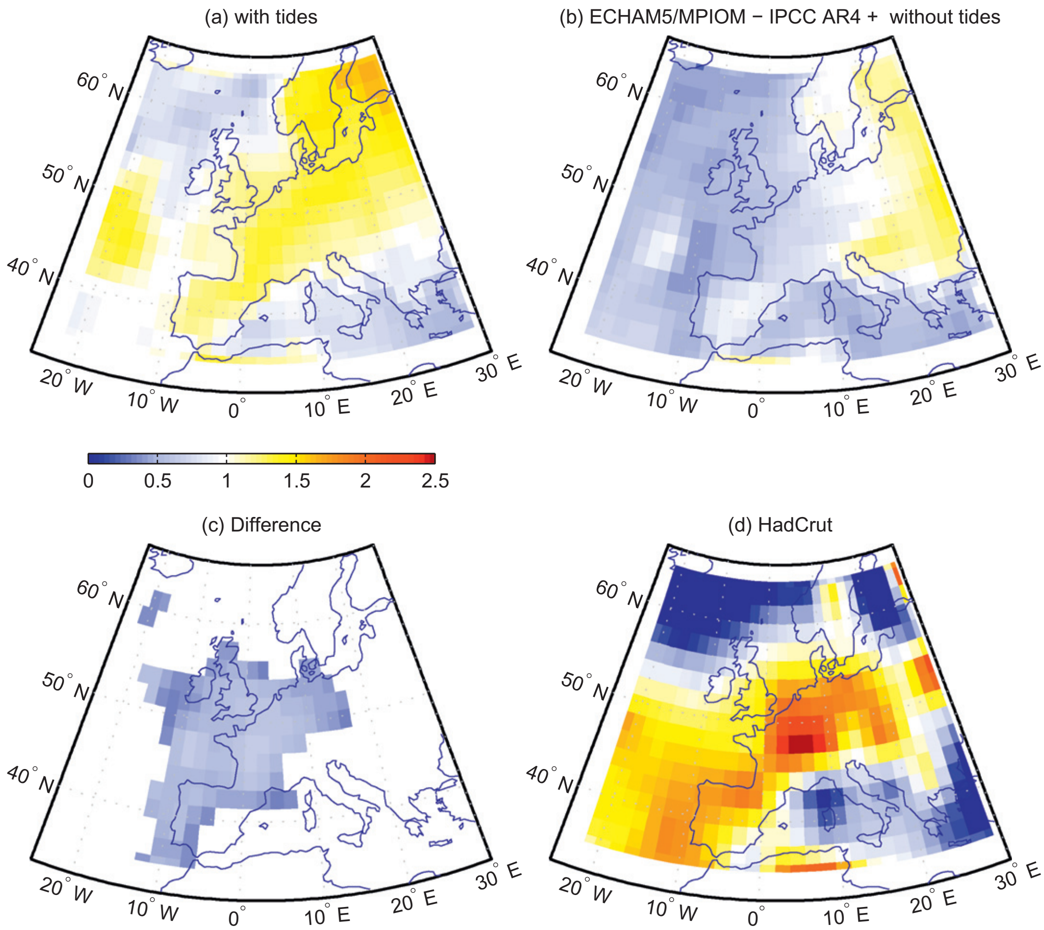

Fig. 12. Temperature trend (1950–2000) defined as a linear regression against the globally averaged temperature anomalies (van Oldenborgh et al., 2009). Mean temperature trend of ensemble of five experiments with tides (a), of three IPCC AR4 simulation of ECHAM5–MPI-OM plus the control run without ocean tides of the present study, and of the HadCrut observational data (d). (c) shows the difference between (a) and (b), only the grid points are displayed where the difference is larger than the standard deviation of (a).

We analyze the temperature trend as a linear regression against the globally averaged temperature anomalies as it is defined in van Oldenborgh et al. (2009). In this sense a trend of value one displays a local temperature trend equal to the global mean temperature trend. The trends over Western Europe are analyzed in the time span from 1950 to 2000 for the five ensemble members of the simulations with tides, the three ensemble members of the IPCC AR4 simulations of the ECHAM5–MPI-OM model plus the simulation without tide, and the HADCRUT3 dataset (Brohan et al., 2006). In Fig. 12 the trends over Wester Europe are shown. The IPCC model results plus the control run without tides show temperature trends over Western Europe lower than the global mean trend. Since van Oldenborgh et al. (2009) were using the same climate model, but different initial conditions and a slightly different time span from 1950 to 2007, their results are similar. The ensemble of the five experiments with tides do show trends of up to 1.5 times the global temperature trend, with the highest values in the northern part of Western Europe. The differences between these two ensembles clearly show that the most significant changes are in regions close to and over the Atlantic Ocean. These results support the hypothesis of van Oldenborgh et al. (2009) that an improvement of the NAC influences the simulation of the Western European Climate. The climate model results for the present temperature trends are closer to the observations when the NAC is improved, but they are still too small. The reason for that could be that the NAC is still not fully corrected in our model with ocean tides. Moreover, van Oldenborgh et al. (2009) mentioned other deficiencies in the climate models likely being responsible for the underestimation of the recent temperature trend in Western Europe.

7. Conclusion

The present study shows that ocean tides have a strong effect on the simulated ocean dynamics. In the ocean model of the present study the simulation of the present state of the North Atlantic becomes more realistic when including tides. This improvement is obtained through the adjustment of the NAC's pathway and consequently by the SST distribution in the North Atlantic. Further, the deep-convection in the Labrador Sea is considerably improved.

Lee et al. (2006) parameterized tidal mixing by allowing for the effect of tidal currents on the Richardson number dependent mixing parameterization. Thus, in their approach tidal mixing is produced in a very similar way to the tidal mixing generated by the explicitly forced tidal currents in our model (Section 4). Since they used a different climate model and found similar improvements of SST in the North Atlantic, it suggests that the described effect of tides on the NAC seems not to be a particular feature of our ocean model. However, the physical mechanism of these changes remains unclear and more sensitivity and idealized experiments will be necessary to analyze and understand the changes of the ocean dynamics in greater detail. The model results and previous model sensitivity studies (Döscher et al., 1994; Gerdes and Köberle, 1995) suggest that the properties of the nordic overflows play a key role in the representation of the NAC and the deep water currents.

The improved pattern of SST in the North Atlantic alters the heat flux between ocean and atmosphere. This lead to an enhanced simulated temperature trend in Western Europe with values getting closer to observational data. The present study support the hypothesis of van Oldenborgh et al. (2009) that the misrepresentation of the NAC in state-of-the-art climate models is to some part responsible for their underestimation of the present temperature trend in Western Europe.

So far, tidal mixing is excited in the model directly, through tidal velocities acting on the vertical mixing scheme of the ocean model. Thus, the tidal mixing is generated in regions of low Richardson numbers (shallow waters). However, it is known that tidal mixing is also excited in the deep ocean (Egbert and Ray, 2000), where the Richardson numbers are large. For future applications it is necessary to implement an additional parameterization, e.g. the internal wave drag from St.-Laurent et al. (2002), in order to allow for tidal mixing in deep ocean regions.

References

Arbic, B., Garner, S., Hallberg, R., Simmons, H., 2004. The accuracy of surface elevations in forward global barotropic and baroclinic tide models. Deep-Sea Res. II 51, 3069–3101.

Arbic, B., Shriver, J., Hogan, P., Hurlburt, H., McClean, J., Metzger, E., Scott, R., Sen, A., Smedstad, O., Wallcraft, A., 2009. Estimates of bottom flows and bottom boundary layer dissipation of the oceanic general circulation from global high-resolution models. J. Geophys. Res. 114.

Arbic, B., Wallcraft, A., Metzger, E., 2010. Concurrent simulation of the eddying general circulation and tides in a global ocean model. Ocean Modell. 32, 175–187.

Bessières, L., Madec, G., Lyard, F., 2008. Global tidal residual mean circulation: does it affect a climate OGCM? Geophys. Res. Lett. 35, L03609.

Böning, C., Bryan, F.O., Holland, W.R., Döscher, R., 1996. Deep-water formation and meridional overturning in a high-resolution model of the North Atlantic. J. Phys. Oceanogr. 26, 1142–1164.

Brohan, P., Kennedy, J., Harris, I., Tett, S., Jones, P., 2006. Uncertainty estimates in regional and global observed temperature changes: a new dataset from 1850. J. Geophys. Res. 111, D12106.

Döscher, R., Böning, C., Herrmann, P., 1994. Response of circulation and heat transport in the North Atlantic to changes in thermohaline forcing in northern latitudes: a model study. J. Phys. Oceanogr. 24, 2306–2320.

Egbert, G., Ray, R.D., 2000. Significant dissipation of tidal energy in the deep ocean inferred from satellite altimeter data. Nature 405, 775–778.

Emery, W., Thompson, R., 1998. Data Analysis Methods in Physical Oceanography. Pergamon Press.

Garrett, C., 2003. Internal tides and ocean mixing. Science 301, 1858–1859.

Gerdes, R., Köberle, C., 1995. On the influence of DSOW in a numerical model of the North Atlantic general circulation. J. Phys. Oceanogr. 25, 2624–2642.

Griffies, M., Pacanowski, R.C., Hallberg, R.W., 2000. Spurious diapycnal mixing associated with advection in a *z*-coordinate ocean model. Mon. Weather Rev. 128, 538–564.

IPCC, 2007. IPCC (Intergovernmental Panel on Climate Change) Climate Change 2007. The Science of Climate Change. Working Group I: The Physical Basis of Climate Change. Cambridge University Press.

Jayne, S.R., 2009. The impact of abyssal mixing parameterizations in an ocean general circulation model. J. Phys. Oceanogr. 39, 1756–1775.

Jungclaus, J., Botzet, M., Haak, H., Keenlyside, N., Luo, J.J., Latif, M., Marotzke, J., Mikolajewicz, U., Roeckner, E., 2006. Ocean circulation and tropical variability in the coupled model ECHAM5/MPI-OM. J. Climate 19, 3952–3972.

Käse, R., Krauss, W., 1996. The Gulf Stream, the North Atlantic Current, and the Origin of the Azores Current. The Warmwatersphere of the North Atlantic Ocean. Gebrüder Borntraeger. pp. 291–337.

Lavender, K., Davis, R.E., Owens, W.B., 2000. Mid-depth recirculation observed in the interior Labrador and Irminger seas by direct velocity measurements. Nature 407, 66–69.

Lee, H.-C., Rosati, A., Spelman, M., 2006. Barotropic tidal mixing effects in a coupled climate model: oceanic conditions in the Northern Atlantic. Ocean Modell. 11, 464–477.

LeProvost, C., 1994. A new in situ reference data set for ocean tides. AVISO Altimetry News Letter 3.

Lyard, F., Lefevre, F., Letellier, T., Francis, O., 2006. Modelling the global ocean tides: modern insights from FES2004. Ocean Dyn. 56, 394–415.

Marsland, S., Haak, H., Jungclaus, J.H., Latif, M., Röske, F., 2003. The Max-Planck-Institute global ocean/sea ice model with orthogonal curvilinear coordinates. Ocean Modell. 5, 91–127.

Montenegro, A., Eby, M., Weaver, A.J., Jayne, S.R., 2007. Response of a climate model to tidal mixing parameterization under present day and last glacial maximum conditions. Ocean Modell. 19 (3–4), 125–137.

Monterey, G., Levitus, S., 1997. Seasonal Variability of Mixed Layer Depth for the World Ocean, vol. 14. NOAA Atlas NESDIS.

Munk, W., Wunsch, C., 1998. Abyssal recipes II: energetics of tidal and wind mixing. Deep-Sea Res. 45, 1977–2010.

Pacanowski, R., Philander, S.G.H., 1981. Parameterisation of vertical mixing in numerical models of tropical oceans. J. Phys. Oceanogr. 11, 1443–1451.

Pickart, R., Straneo, F., Moore, G.W.K., 2003. Is Labrador sea water formed in the Irminger Basin? Deep-Sea Res. I 50, 23–52.

Ray, R.D., 2001. Inversion of oceanic tidal currents from measured elevations. J. Mar. Syst. 28, 1–18.

Roeckner, E., Bäuml, G., Bonaventura, L., Brokopf, R., Esch, M., Giorgetta, M., Hagemann, S., Kirchner, I., Kornblueh, L., Manzini, E., Rhodin, A., Schlese, U., Schulzweida, U., Tompkins, A., 2003. The atmospheric general circulation model ECHAM5. Part i: model description. Tech. Rep., Max Planck Institute for Meteorology.

Saenko, O.A., 2006. The effect of localized mixing on the ocean circulation and time-dependent climate change. J. Phys. Oceanogr. 36, 140–160.

Schiller, A., 2004. Effects of explicit tidal forcing in an OGCM on the water-mass structure and circulation in the Indonesian throughflow region. Ocean Modell. 6, 31–49.

Schiller, A., Fiedler, R., 2007. Explicit tidal forcing in an ocean general circulation model. Geophys. Res. Lett. 34, L03611.

Shum, C., Woodworth, P.L., Andersen, O.B., Egbert, G., Francis, O., King, C., Klosko, S.M., Provost, C.L., Li, X., Molines, J.-M., Parke, M.E., Ray, R.D., Schlax, M.G., Stammer, D., Tierney, C.C., Vincent, P., Wunsch, C.I., 1997. Accuracy assessment of recent ocean tide models. J. Geophys. Res. 102, 25173–25194.

Simmons, H.L., Jayne, S.R., Laurent, L.C.S., Weaver, A.J., 2004. Tidally driven mixing in a numerical model of the ocean general circulation. Ocean Modell. 6, 245–263.

St.-Laurent, L.C., Simmons, H.L., Jayne, S.R., 2002. Estimating tidally driven mixing in the deep ocean. Geophys. Res. Lett. 29, 2106.

Steele, M., Morley, R., Ermold, W., 2001. A global ocean hydrography with a high quality Arctic Ocean. J. Climate 14, 2079–2087.

Thomas, M., Sündermann, J., Maier-Reimer, E., 2001. Consideration of ocean tides in an OGCM and impacts on subseasonal to decadal polar motion excitation. Geophys. Res. Lett. 28, 2457–2460.

Valcke, S., 2006. OASIS3 user guide (prism_2-5). Tech. Rep., PRISM Support Initiative.

van Oldenborgh, G., Drijfhout, S., van Ulden, A., Haarsma, R., Sterl, A., Severijns, C., Hazeleger, W., Dijkstra, H., 2009. Western Europe is warming much faster than expected. Climate Past 5, 1–12.

Weese, S., Bryan, F.O., 2006. Climate impacts of systematic errors in the simulation of the path of the North Atlantic Current. Geophys. Res. Lett. 33.

Zahel, W., Gaviño, J.H., Seiler, U., 2000. Angular momentum and energy budget of a global ocean tide model with data assimilation. GEOS 20, 400–413.